Book of Tutorials and Abstracts

European Microbeam Analysis Society

EMAS 2024

14th

REGIONAL WORKSHOP

on

THE EDGE OF NEW EM AND MICROANALYSIS TECHNOLOGY

12 to 15 May 2024
at the
Brno University of Technology, Brno, Czech Republic

Organised in collaboration with:
Brno University of Technology (VUT)
Central European Institute of Technology (CEITEC)

EMAS
European Microbeam Analysis Society eV
www.microbeamanalysis.eu/

This volume is published by:
European Microbeam Analysis Society eV (EMAS)
EMAS Secretariat
c/o Eidgenössische Technische Hochschule, Institut für Geochemie und Petrologie
Clausiusstrasse 25
8092 Zürich
Switzerland

ISBN 978 90 8227 6978
NUR code: 971 – Materials Science

INTRODUCTION TO SEM

Ivo Kuběna

Institute of Physics of Materials
Zizkova 22, Brno, Czech Republic
e-mail: kubena@ipm.cz

Dr Ivo Kuběna obtained in 2008 his Engineering degree from the Brno University of Technology. After research at the Institute of Physics of Materials of the Czech Academy of Sciences, he obtained his PhD in 2012 from the Brno University of Technology. Subsequently, he held a junior researcher position at Institute of Physics of Materials of the Czech Academy of Sciences. This was followed by a visiting researcher position at the Paul Scherrer Institute in Villigen, Switzerland. Later on became the head of the service "Electron Microscopy" group of the Institute of Physics of Materials of the Czech Academy of Sciences. At present he is head of the scientific "Low Cycle Fatigue" group with a focus on analysis of the relation of material microstructure and fatigue properties, SEM and TEM analyses and data evaluation and interpretation. He is (co-) author of 85 peer-reviewed publications.

1. INTRODUCTION

The first microscopes using light as the emission source were constructed more than 400 years ago. The optical system evolved through ages and system defects were corrected or even removed. However, there was always a limitation in the observed objects size. The physical limit of light microscopy was derived by Abbe and Airy and is given by Eq. (1):

$$d_d = 0.61\lambda/\alpha \tag{1}$$

where d_d is the spatial resolution, λ is the wavelength of the used probe (visible light), and α is the aperture angle. Knowing the λ for visible light (~390 - 760 nm), it can be said that spatial resolution lies in the low hundreds of nm and this limit cannot be overcome. Therefore, to reveal smaller features, for example the internal structure of engineering materials predetermining their properties, another source of emission had to be found. Due to the much smaller wavelength, small mass, electric charge and relative gentle interactions with specimens, electrons were chosen for new emission sources.

The scanning electron microscopy (SEM) became an irreplaceable tool in many fields of the (not only) material research. The attractivity of the SEM stems from its capability to observe various materials over a wide magnification range 10× - 100,000×, with a spatial resolution around or even better than 1 nm. Once the electron hits the specimen, following signals are emitted and can be detected: Secondary electrons (SE), backscattered electrons (BSE), Auger electrons (AE), cathodoluminescence (CL), and characteristic and continuous X-rays. The electrons may go through sufficiently thin specimens and transmitted, diffracted and scattered electron can be detected.

Theoretical values of electron wavelength depending on accelerating voltage can be calculated from Eq. 2:

$$\lambda = \frac{h}{\sqrt{2m_0 eU\left(1+\frac{eU}{m_0 c^2}\right)}} \sim \frac{h}{\sqrt{2m_0 eU}} \sim \frac{1.226}{\sqrt{U}} \tag{2}$$

where h is Planck constant, m_0 is invariant (rest) mass and U is accelerating voltage. It should be noted that a relativistic correction is necessary. When the estimated wavelength is used for the calculation of spatial resolution d_d by Eq. 1, the theoretical spatial resolution of SEM with an acceleration voltage of 10 kV is less than 0.01 nm, which is much better (almost two order of magnitude) than the spatial resolution in commonly used SEM. The deterioration of spatial resolution lies in the imperfection of the microscope optical system. Each lens and aperture suffer by optical aberrations such as coma, chromatic and spherical aberrations and astigmatism. Later developments in precise machining reduced optical aberration significantly allowing to reach a higher spatial resolution, but still far from the theoretical one.

The first observation of thick specimens by SEM is dated to year 1942. Zworykin *et al.* [1] proved that the SE's are responsible for the topographic contrast. The next important step was the improvement of SE detector by Everhart and Thornley (E-T) [2] in 1960, who employed a scintillator to convert electron to light, which is further transmitted to a photomultiplier. It resulted in significant signal to noise ratio improvement. E-T detectors are still present in SEM chambers. The BSE detectors were slightly delayed and they were proven to carry information about atomic number as shown for example by Heinrich in 1966 [3]. It means that the combination of SE and BSE signals can provide very large amount of information about the specimen surface and its phase composition. In order to determine the phase composition also qualitatively, energy-dispersive X-ray spectrometry (EDS) and electron backscattered diffraction (EBSD) techniques are adopted. EBSD allows also the characterisation of material's crystallographic texture and can be used for grain size determination. The reader is kindly referred to [4-14] for more detailed information.

2. SAMPLE

As an example of the SEM, EDS and EBSD possibilities in material development, the results obtained IN939 superalloy are shown. The IN939 was prepared in two variants: By conventional casting and by additive manufacturing (AM), namely by laser powder bed fusion (L-PBF). Three steps heat treatment was performed to obtain the final microstructure, which is strengthened by coherent γ'-precipitates. The powder and the resulting microstructure were described and the main differences between conventional and 3D printed AM material were addressed. Subsequently, the influence of microstructure on cyclic stress strain curve was measured and discussed.

3. EXPERIMENT

The nickel-based superalloy IN939 with a nominal composition of 22.5 Cr, 19.1 Co, 3.7 Ti, 2.0 W, 2.0 Al ,1.4 Ta, and 1.0 Nb (in wt%) and Ni for balance, prepared by conventional casting and laser powder bed fusion (L-PBF), was investigated.

Detailed analysis of the microstructural features and their evolution using SEM. A TESCAN LYRA 3 XMU FEG/SEM x FIB equipped with an EDS system (model X-Max 80, Oxford Instruments) was used to analyse the experimental material's microstructure. EBSD was adopted to analyse grain size and crystallographic texture of the material after production. In characterizing the grain distribution, the high angle grain boundaries were counted if the disorientation angle was greater than 15°.

SEM was used for analysis of the powder used for the material's preparation as well as for the microstructural analysis of the prepared material. Both the bulk material specimens as well as the powders were conventionally mounted in a conductive polymer. The microstructure of the experimental material was characterised on metallographic specimens prepared by grinding on SiC papers and mechanical polishing by diamond paste (1 µm) using ethanol as lubricant and polishing by a water-based colloidal silica suspension containing particles with a 0.04 µm size. A mixture of 4.9 $HClO_4$ + 95.1 CH_3COOH at 8 °C was used for electropolishing of the specimens before EBSD analysis. To visualise the microstructure an aqueous solution of 10 % $C_2H_2O_4$ was used.

4. RESULTS

Two variants of the IN939 alloy, a cast one and its L-PBF treated counterpart, were exposed to three steps of heat treatment consisting of *i*) solution annealing at 1,175 °C/45 min, *ii*) precipitation hardening at 1,000 °C/6 h, and *iii*) finally at 800 °C/4 h.

At first, the commercially purchased IN939 powder was investigated using SEM. A typical micrograph of the IN939 powder is shown in Fig. 1. The remainder of the particles, not stuck on the tape, had to be removed before inserting the holder into SEM. The powder size varies over a range between 40 and 60 µm; only a small fraction of the powder consists of smaller particles of about 10 µm. Image analysis software was used to determine the powder size and distribution. The powder particles do not exhibit cracks or voids or other non-homogeneities.

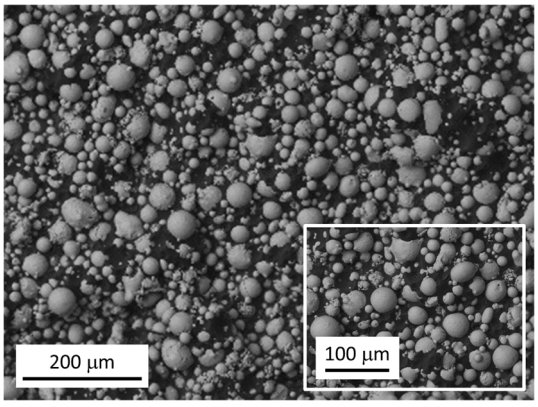

Figure 1. BSE image of IN939 powder; 15 kV.

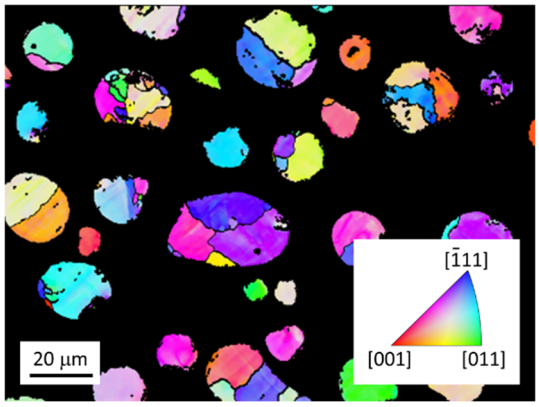

Figure 2. EBSD image of IN939 powder; 20 kV, step size 0.5 µm.

The cross-section of the powder particles mounted in the conductive resin after metallographical preparation was investigated by EBSD. Preparation of the specimen had to careful since the powder particles tend to fall off during grinding and polishing and also due to the small size of

the particles. Also, electrolytic etching was responsible for partial powder particles removal from the metallographic tablet. EBSD revealed that the single powder particle is not a monocrystalline, but consist of several, randomly oriented grains (Fig. 2). Moreover, no internal defects in powder particles were detected. The analysis of the cross-section of the powder particles should not be considered for particle size characterisation as the particles were ground to a different extend and the revealed size is not representative, not even their shape as it is influenced by the hot mounting and mechanical preparation.

The microstructure of conventionally cast IN939 is shown in Fig. 3. Polyhedral dendritic grains with an average size of 0.9 ± 0.3 mm and a relatively high amount of casting defect of sizes up to 0.3 mm were observed. The average grain size was determined by applying the linear intersection method. A large number of metal-carbide (MC) enriched by Ti, Ta and Nb are located at the grain boundaries as revealed by BSE imaging (Fig. 4). No crystallographic texture was observed by the EBSD analysis.

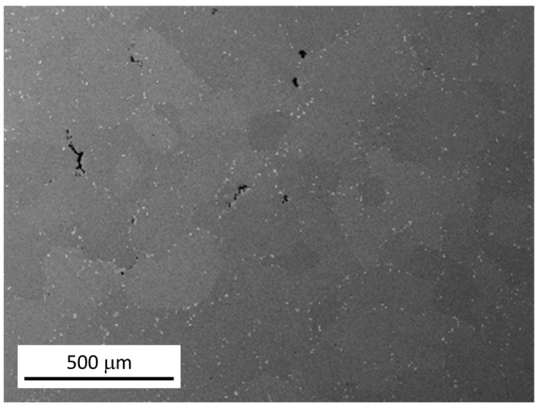

Figure 3. BSE image of polyhedral grains of cast IN939; 10 kV.

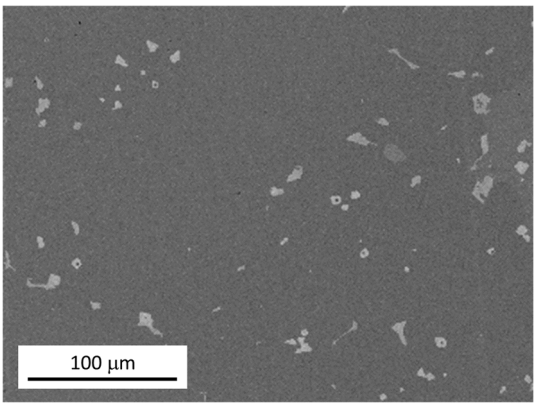

Figure 4. BSE image of carbides observed at grain boundaries in cast IN939; 10 kV.

The microstructure of the as-built L-PBF IN939 consists of grains elongated in the building direction (BD). The grain size in the section perpendicular to the building direction was determined as 13.39 ± 11.43 µm (Fig. 5), while the length of the grain in the building direction was around 100 µm (Fig. 6), which means that aspect ratio about 10. Due to the specific grain shape, a MATLAB-script was written for the grain size determination. Moreover, strong <001> crystallographic texture in the building direction was revealed by EBSD in the direction parallel to the BD as shown in the Fig. 7.

The microstructure cannot be considered as homogeneous, mainly due to the significant difference in the grain size in BD and in direction parallel to BD as well as due to the strong texture in the direction parallel to BD resulting in anisotropy of properties.

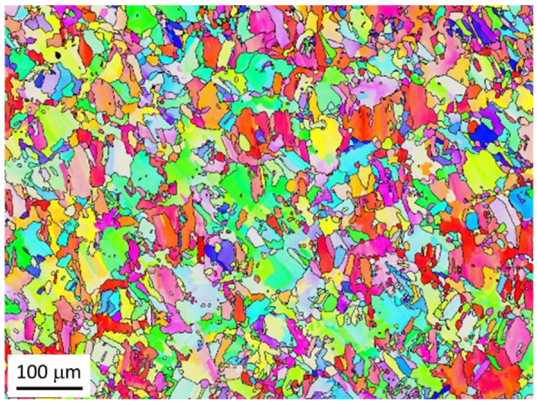

Figure 5. EBSD grain orientation map of L-PBF IN939, perpendicularly cut to BD; 20 kV.

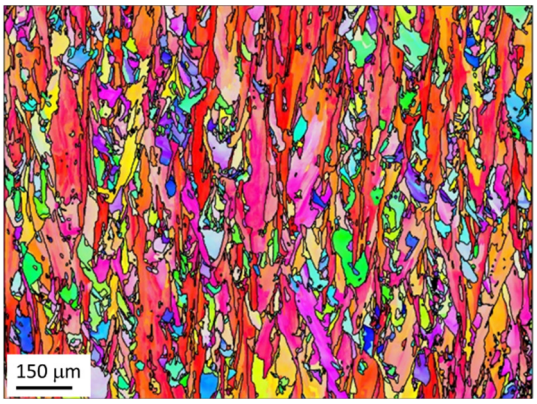

Figure 6. EBSD grain orientation map of L-PBF IN939, parallel cut to BD; 20 kV.

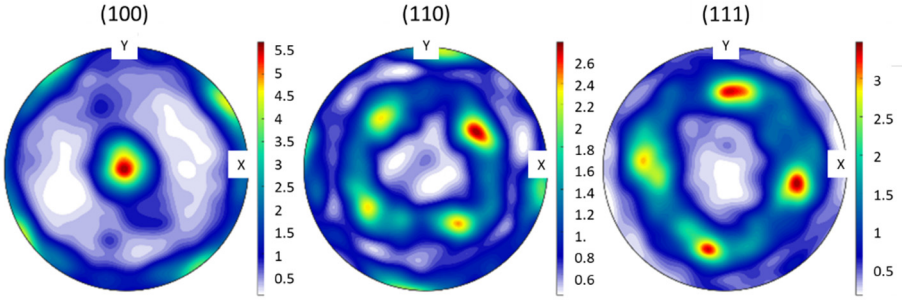

Figure 7. Pole figures of the crystallographic texture parallel to the BD.

Both variants of the IN939, a cast one and its L-PBF treated counterpart, were exposed to a three steps heat treatment consisting of solution annealing and precipitation hardening. Coherent precipitates exhibit bimodal distribution, on the one hand large precipitates with a size of about 180 nm and on the other hand small precipitates with a size of about 10 nm as shown in Fig. 8 for the L-PBF IN939. Surprisingly, the precipitate size distribution was the same for both variants of the IN939.

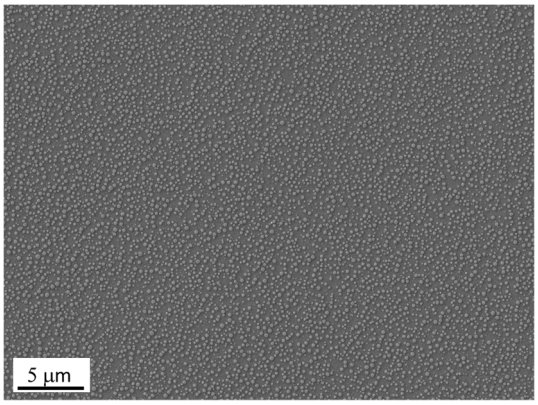

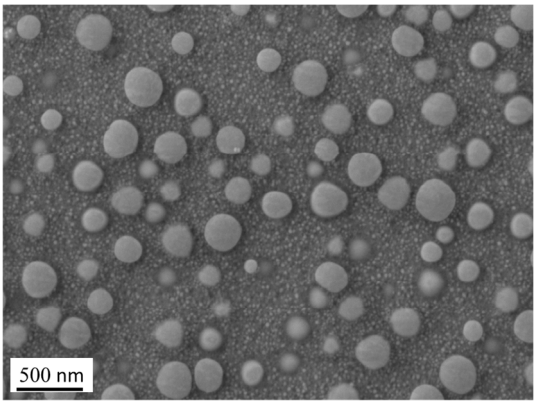

Figure 8. An overview of the large precipitate distribution after heat treatment (left) and a detail (right) showing the smaller precipitates, in L-PBF IN939; BSE, 10 kV.

5. CONCLUSION

The importance SEM analysis in material research, namely for microstructural analysis of IN939 alloy is obvious. Following conclusion can be drawn:

- Polyhedral grains with a size of 0.3 - 0.9 mm, dendritic structure and casting defect were revealed in IN939 prepared by conventional casting. No texture of the structure was observed.
- The elongated grains in building direction and crystallographic <001> texture were revealed in the microstructure of IN939 prepared by L-PBF, which will have a direct impact on material's response to the loading.
- The same bimodal particle distribution was observed after a three steps heat treatment, regardless of the preparation route.

6. REFERENCES

[1] Zworykin V K, Hiller J and Snyder R L 1942 *ASTM Bull.* **117** 15
[2] Everhart T E and Thornley R F M 1960 *J. Sci. Instr.* **37** 246
[3] Heinrich K F J 1968 *Science* **159** 528
[4] Cosslett V E and Duncumb p 1956 *Nature* **177** 1172
[5] Danilatos G D 1991 *J. Microscopy* **162** 391
[6] Fitzgerald R, Keil K and Heinrich K F J 1968 *Science* **159** 528
[7] Goldstein J I, *et al.* 1976 *Scanning electron microscopy and X-ray microanalysis.* [New York, NY: Springer]
[8] Goldstein J I, *et al.* 2018 *Scanning electron microscopy and X-ray microanalysis. Fourth edition*. [New York, NY: Springer] 550 pp.
[9] Hiller J 1947 U.S. Patent No. 2,418,029
[10] Knoll M 1935 *Z. Tech. Phys.* **11** 467
[11] Kyser D F and Wittry D B 1966 in: *The electron microprobe*. [New York, NY: Wiley] 691
[12] Long J V P and Agrell S O 1965 *Mineralogical Mag.* **34** 318
[13] Oatley C W and Everhart T E 1957 *J. Electron.* **2** 568
[14] Wells O C 1959 *J. Electron. Control.* **7** 373